ACS Catalysis, Volume 8, Issue 11, 2018, pp. 10164-10172
DOI: 10.1021/acscatal.8b02409

In-Situ Tuning of Catalytic Activity by Thermoelectric Effect for Ethylene Oxidation

Abdenour Achour [+], Jian Liu [%], Ping Peng [%],

Christopher Shaw [+] and Zhaorong Huang [+*]

[+] Surface Engineering and Precision Institute, Cranfield University, Bedfordshire MK43 0AL, UK

[%] School of Materials Science & Engineering, Hunan University, Changsha 410082, China

Published by American Chemical Society. This is the Author Accepted Manuscript issued with: Creative Commons Attribution Non-Commercial License (CC:BY:NC 4.0). The final published version (version of record) is available online at DOI:10.1021/acscatal.8b02409. Please refer to any applicable publisher terms of use.

ABSTRACT

The use of the thermoelectric material BiCuSeO as a support and promoter for catalytic ethylene oxidation is reported here. The catalytic activity of a continuous and non-continuous Pt catalyst supported on BiCuSeO was observed to be promoted significantly by an *in-situ* generated thermoelectric Seebeck voltage by the temperature difference across the material. It has also been shown that this promotion of catalysis by thermoelectric effect enabled the material BiCuSeO itself to be highly catalytically active for ethylene oxidation. A linear relationship between the logarithm of the reaction rate and the thermoelectric Seebeck voltage was also observed. The thermoelectric promotion of catalysis is attributed to the change of work function of the catalyst surface, accompanied by a charge transfer from the bulk to the surface due to the thermoelectric effect.

KEYWORDS: thermoelectric materials; promotion of catalysis; electrochemical energy; work function; ethylene oxidation

▪ INTRODUCTION

It is highly attractive to be able to tune the catalytic activity under operation of a system, particularly for operations under dynamic conditions. [1] Generally this can be achieved by tuning the particle size of the active component *in-situ*, [2,3] or introducing promotional species onto the catalyst surface by applying an external small current or voltage to the metal catalysts supported on solid state electrolyte, through non-Faradaic electrochemical modification of catalytic activity (NEMCA). [4-9] NEMCA has been observed in many catalytic chemical reactions but its practical industrial use is rare. This is because it requires the catalyst (often expensive noble metals) to be an continuous electrode to maintain electrical connection under often harsh chemical reaction conditions, the efficiency of catalytic materials is very low. [10,11] To overcome these shortcomings of the NEMCA technique, recently the concept of self-sustained electrochemical promotion of catalysis and the use of mixed ionic electronic conducting electrode has been reported.[11-13]

A novel method to tune catalytic activity *in-situ* has been reported recently by using thermoelectric (TE) materials as a catalyst support and promoter. It was reported that the CO_2 hydrogenation and CO selectivity on Pt catalysts supported on a TE material BiCuSeO ceramics was increased significantly when there was a large temperature difference across the TE material, and the phenomenon was called thermoelectric promotion of catalysis (TEPOC).[14] TE materials convert a temperature gradient into electrical voltage via the Seebeck effect, $S= -V/\Delta T$, here S is called the Seebeck coefficient, ΔT is the temperature difference across the TE material, and V is the voltage. The oxyselenide BiCuSeO (BCSO) was used as the TE material for its low

thermal conductivity (<0.5 $Wm^{-1}K^{-1}$) so that a large temperature gradient can be established easily across the material. It also has a high Seebeck coefficient which enables the generation of a large Seebeck voltage, and high temperature stability with no decomposition below 773 K .[15-21] It was further observed that there exists a linear relationship between the logarithm of the reaction rate and the ratio $-eV/k_bT_h$ (a dimensionless parameter), i.e.

$$Ln(r/r_0) = -\gamma eV/k_bT_h \qquad (1)$$

where γ is a dimensionless positive constant, -e the charge of an electron, k_b the Boltzmann constant, r_0 is the reaction rate without any Seebeck voltage, i.e. when $T_c=T_h$, T_c and T_h are the temperatures at the cold and hot surface of the TE material.[14]

The TEPOC was interpreted by assuming that the work functions of the catalyst Pt and also the thermoelectric material BCSO were changed by the Seebeck energy – eV, [14] as it has been established that a change of work function of a catalyst will lead to the exponential change of its catalytic activity. [22] The general nature of the mechanism suggests that TEPOC may be a universal phenomenon. It is therefore of paramount importance to demonstrate that TEPOC can also be observed in other catalysed chemical reactions. For this purpose, ethylene oxidation has been chosen as the model reaction in this work. Ethylene oxidation on platinum has been extensively investigated before, because this reaction has been used in automotive exhaust catalyst converters, and the reaction mechanisms were well understood.[4,5,23] Other benefits were that the forward reaction products include carbon dioxide CO_2 which is very stable, and the reverse reaction was very hard to take place, so it can often be ignored when considering the whole process.[24]

▪ EXPERIMENTAL SECTION

Thermoelectric materials preparation. The TE material BiCuSeO (BCSO) was produced by using a B_2O_3 flux solid-state reaction method. A cold press system was used to form a dense disc of 20 mm in diameter and 2 mm in thickness, followed by sintering in argon atmosphere at 923 K for 10h. Further details can be found in previous publications.[14, 25] For the solid electrolyte, the dense Yttria-stabilized zirconia (YSZ) discs were prepared from 8 mol% YSZ (CoorsTeK powder, 99.99%; average grain size, 0.5-0.7 μm), and sintered at 1773 K for 2 hours in air (achieved density higher than 98%). YSZ discs were 16 mm in diameter and 1.5 mm in thickness. The composite discs of $(BiCuSeO)_{0.9}(YSZ)_{0.1}$ were synthesized by mixing commercial YSZ powders and lab prepared BiCuSeO powders in ethanol. The composite suspension was homogenized in ultrasonic for ~ 30 minutes, followed by ball milling for 24 hours with a zirconia milling balls to powder weight ratio of 5:1. The ethanol solvent was evaporated in an oven (Memmert model UNE 300) with enforced air circulation. The resulting powders were compacted at 150 MPa using a hydraulic press system. The above prepared discs were then sintered in argon at 923 K for 10 hours. Scanning electron microscopy (Philips XL30 S-FEG) and X-ray diffraction (Siemens D5005) techniques were employed for structural and compositional characterisation.

Pt catalysts preparation. A number of Pt catalyst systems were investigated. Thin films of Pt catalyst with nominal thickness 80 nm were deposited on the one side of the BCSO disc in Argon atmosphere at room temperature, and referred to as Pt(80)/BCSO. Further details of the Pt films, with nominal thickness of 15 and 80 nm,

can be found in the previous publication.[14] All the BCSO, Pt(80)/BCSO and Pt(15)/BCSO discs weighed 5.8g.

Pt nanoparticle containing samples (Pt(NP)/BCSO) were prepared by mixing BCSO powders with a solution of H_2PtCl_6 (Sigma-Aldrich, 8wt% in water), using ultrasonic agitation at 313 K for 60 min. The excess water was evaporated overnight at 383 K, and finally the green disc was formed using cold pressing, and calcined at 823 K for 1 hour under argon. This sample also weighed 5.8g.

For NEMCA investigation, electrodes were prepared by sputtering of noble metals onto the disc samples of YSZ. Platinum was used as the catalyst and working electrode (WE), and was deposited on one side of a pellet by DC magnetron sputtering, whilst gold (Au) as the counter and reference electrodes were deposited on the other side by RF magnetron sputtering. The working and counter electrodes were located in a symmetrical face-to-face arrangement on the opposite sides of the disc, in a configuration typical for carrying out NEMCA testing. This sample is referred to as Pt(80)/YSZ. A 80 nm thin film of Pt catalyst deposited on a composite pellet of 90%wt BiCuSeO and 10%wt YSZ was prepared similarly (weight 5.02g) and was coded as $Pt(80)/(BiCuSeO)_{0.9}(YSZ)_{0.1}$.

The reaction chamber. The chamber reactor (**Figure S1a**) which can combine thermoelectric effect with catalytic chemical reaction has been described in detail in a separate publication.[14] Briefly, the reactor consisted of a stainless steel cylinder of 40 cm^3 in volume capped with a cover plate that was sealed with an O-ring and secured by screws. The cover plate was cooled with running water. The reactor was sitting on a hotplate, with gold wires and thermocouples led out of the reactor chamber through

two four-hole alumina clad tubes (Omega, Omegatite 350). A disc sample was placed into a specific glass ceramic holder (MACOR) and attached to the cooling surface of the cover plate for normal thermoelectric effect experiments. Gold wire was selected because of its minimal catalytic activity, as verified through blank control experiments. In order to eliminate artefacts, gas leaks were carefully monitored throughout the progress of experiments. The Seebeck voltage, or catalyst potential difference according to the procedure generally used in conventional NEMCA three-electrode electrochemical cells, were measured using a potentiostat-galvanostat (VersaStat 3F, Princeton Applied Research) between the bottom hot and upper cold surfaces, or between the working electrode (Pt) and the reference electrode (Au).

Chemical reaction characterisation. The chemical reactions were carried out under atmospheric pressure, and the schematic of the experimental set-up is shown in **Figure S1b**. A set of three gas mass flow controllers (MFCs) was used to control the gas composition and flow rate. The reactant gases were BOC certified standards of O_2 (99.996%) supplied as a 20% mixture in He (99.996%), and 4% C_2H_4 mixture in He (99.996%), with helium (BOC, 99.996%) being used as a carrier gas to obtain the desired concentrations. The overall flow rate was 200 mL min^{-1} and the reactive mixture was composed of ethylene with partial pressure $P_{C_2H_4}$ = 0.189 kPa and oxygen with partial pressure P_{O_2} = 3.01 kPa. For the structure stabilization, the Pt film was pre-treated in 5% H_2/Ar at 603 K for 2 h in order to reduce the platinum, before the sample was cooled down to room temperature under the flow of helium. The sample was pre-treated at 723 K for 4h under the reaction mixture. Finally, the temperature was decreased to room temperature for catalytic activity measurements.

Inline Gas Chromatography (GC8340, CE instruments) was used to quantify the concentration of reactants and products C_2H_4, O_2 and CO_2, and in-line IR analyzer (G150 CO_2, Gem Scientific) was used to double check the concentration of CO_2. The gas chromatograph (GC) was equipped with a Thermal Conductivity Detector (TCD) and two columns, containing Molecular Sieve 5A and a Porapak Q respectively. Data acquisition and manipulation were performed using the TotalChrom Workstation (Version 6.2.1 for Windows) data system. Each measurement was repeated three times to test the stability and reproducibility. At each temperature, the catalyst was allowed to reach a steady state for 20-30 min and then three GC injections and measurements were performed. The average of three GC measurements at each temperature is reported. Blank testing of the empty reactor and all samples were performed in the temperature range of 300 – 723 K. It is noteworthy to mention that the carbon mass balance was found to be within 6% for all experiments.

The reactions were evaluated using the rate of carbon dioxide production and ethylene conversion from the outlet partial pressures of C_2H_4 and CO_2, according to the stoichiometry of the reaction:

$$C_2H_4 + 3\ O_2 \longrightarrow 2\ CO_2 + 2\ H_2O \qquad (6)$$

Carbon dioxide was the only observed product and its partial pressure at the outlet was converted to area specific molar flow rate in $nmols^{-1}$ by using the following equation:

$$r_{CO_2} = \frac{(Pco_2/101.3)}{22400 \text{ x } 60} \text{ x } f_v \text{ x } 10^9 \qquad (7)$$

where f_v is the volumetric flow rate at the outlet of the reactor in ml min^{-1}. The rate of consumption of O (r_o) was simply:

$$r_o = 3 \text{ x } r_{CO_2}$$

The ethylene conversion into CO_2 was defined as:

$$\%\ C_2H_4 \text{ Conversion} = \frac{Pco_2}{Pco_2 + 2\ P_{C_2H_4}} \text{ x } 100 \qquad (8)$$

where Pco_2 and $P_{C_2H_4}$ were the partial pressure of CO_2 and C_2H_4 in the outlet, respectively.

▪ RESULTS AND DISCUSSION

Microstructure of the catalyst system. Scanning electron microscopy (SEM) surface morphology images for the samples Pt(80)/BCSO, Pt(15)/BCSO, Pt(80)/$(BiCuSeO)_{0.9}(YSZ)_{0.1}$ and BCSO after they have been subjected to catalytic reaction experiments are shown in **Figure 1a-d**. It can be seen that the BCSO had grain size between 2 and 8 μm, with a very clean surface (**Figure 1a**). For the Pt(15)/BCSO, small Pt particles on the surface of BCSO grains (indicated by arrow heads) were observed (**Figure 1b**). For Pt(80)/BCSO (**Figure 1c**), more and larger Pt particles were observed (indicated by arrow heads). 80 nm was deemed the minimum Pt thickness to ensure electrical conductivity on the surface of the YSZ. Pt(80)/$(BiCuSeO)_{0.9}(YSZ)_{0.1}$ consisted of relatively large BCSO grains and much smaller (~ 0.1 μm) YSZ grains (**Figure 1d**). **Figure 1e** shows X-ray diffraction (XRD) patterns for the above samples. Apparently, BCSO was a single phase (PDF#45-0296) in every sample, no second phase was observed. Strong Pt peak can be observed for all the samples with a 80 nm Pt film. However, no Pt peak could be seen for Pt(15)/BCSO, suggesting the Pt grain size in the Pt(15)/BCSO was beyond the XRD detection limit, and therefore existed as separate nano-particles.

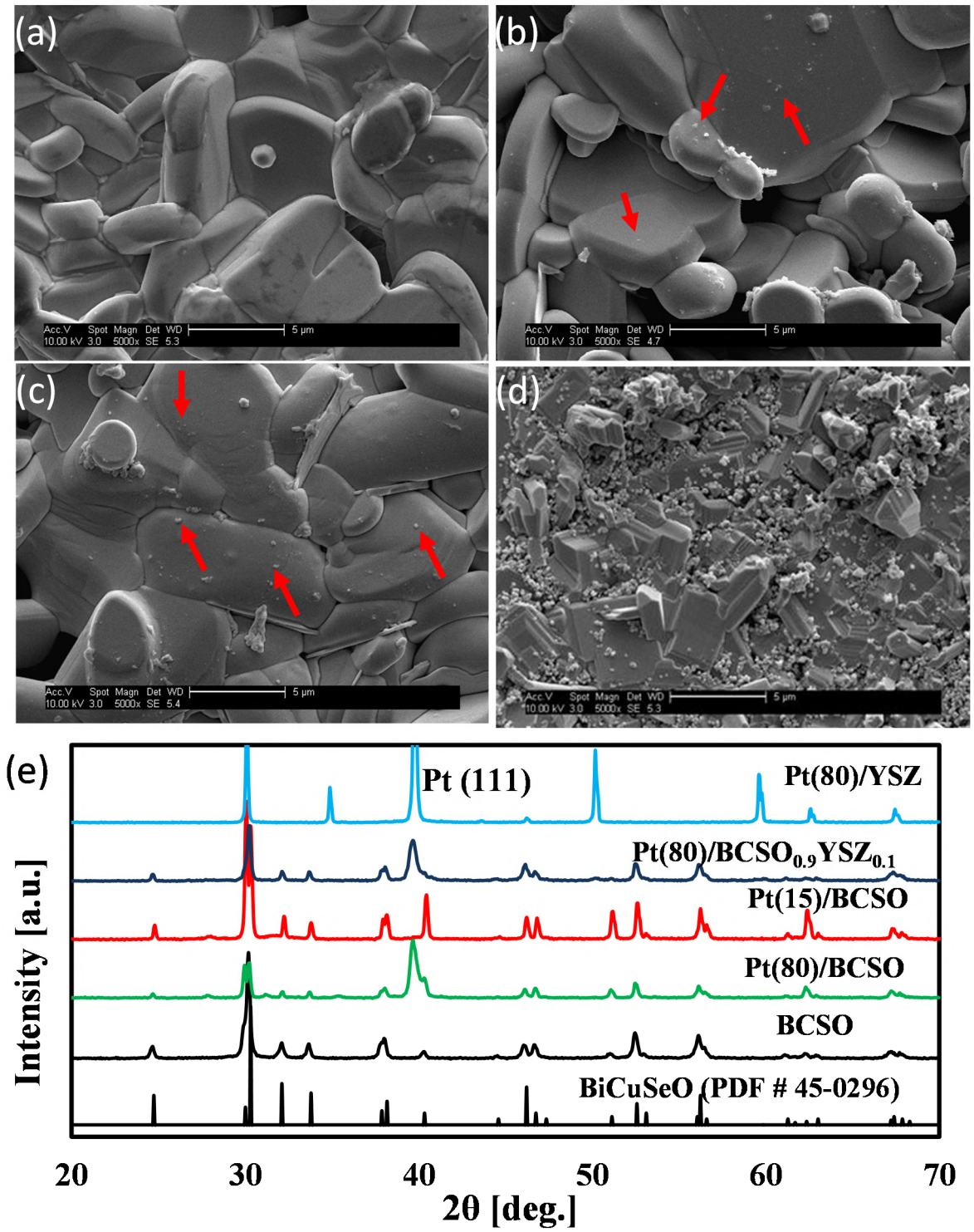

Figure 1. Surface SEM images of catalyst systems after catalytic chemical reaction characterisation: (a) bare BCSO; (b) Pt(15)/BCSO; (c) Pt(80)/BCSO; (d) Pt(80)$(BiCuSeO)_{0.9}(YSZ)_{0.1}$. BCSO grains were much larger than YSZ grains; (e) XRD patterns for all samples and Pt(80)/YSZ. The arrow heads point to Pt particles.

Substantial higher catalytic activity for Pt catalysts supported on TE materials with a Seebeck voltage. The reaction chamber was heated by a hot-plate, and its top cap is water cooled (for details see **Figure S1 and Figure S2**). A disc sample of 20 mm in diameter and about 2 mm in thickness was then placed into a specific glass ceramic holder and attached to the cold surface of the cap for catalytic reaction investigation under the TE conditions. As the back side of the disc was in contact with the water cooled stainless steel cap, its temperature was always less than 373 K (**Table S1**). When the front surface of the disc was at a high temperature, a large temperature difference was created between the hot surface T_h and cold surface T_c, hence a high Seebeck voltage was generated. At the reduced TE (RTE) condition, the back surface T_c of the disc was not in direct contact with the cap, therefore the temperature difference across the disc thickness and also the Seebeck voltage were much smaller.

Figure 2 shows the ethylene oxidation reaction rates for different front surface temperatures T_h for Pt(80)/BCSO with a large TE effect (Pt(80)/BCSO TE), and under a reduced TE effect (Pt(80)/BCSO RTE) respectively. For Pt(80)/BCSO TE, when the front surface T_h was at 666 K, the backside temperature T_c was 349 K, so a temperature difference of 317 K existed across the BCSO thickness, which generated a Seebeck voltage -71 mV (more details in **Table S1**). The corresponding reaction rate of oxygen was measured as 2258 $nmols^{-1}$ and the conversion of C_2H_4 was 99.9% for the flow rate used within these studies (more details in **Figure S3**). For the same sample under the RTE conditions (Pt(80)/BCSO RTE) at 553 K (more details in **Table S2**), the measured Seebeck voltage was -3.1 mV, and the reaction rate was only 0.08 $nmols^{-1}$. These values for the RTE case became -8.6 mV, 7.1 $nmols^{-1}$ and 1.2% respectively, when the hot surface T_h was increased to 713 K. This

highlights, that for the same sample, the reaction rate under the TE condition at 666 K was 318 times greater than the rate observed under the RTE condition at a higher temperature of 713 K. For better comparison with the TE case, the rate under RTE conditions was interpolated for the same temperature of 666 K and the new estimated ratio of reaction rates between the TE and RTE conditions was found to be 660. It is plausible to assume from this that if the temperature gradient could be fully removed in the RTE case then the observed Seebeck voltage effect on this ratio would be even higher. The above experiments have been repeated at least once and the results have been shown to be reproducible, which helps to rule out the possibility that the rate difference was due to particle aggregation at the surface. The same samples were used for reported CO_2 hydrogenation studies. [14]

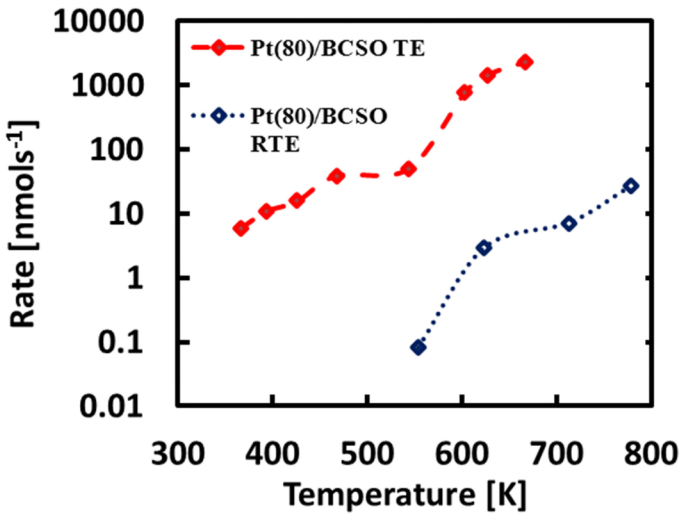

Figure 2. Ethylene oxidation rates as functions of temperature at the catalyst surfaces, for Pt(80)/BCSO under large TE effect (Pt(80)/BCSO TE) and reduced TE effect (RTE) conditions. Much higher Seebeck voltages were generated across the thickness of the catalyst support BCSO under TE than under RTE conditions. Notice the logarithm scale for rate.

Seebeck voltage alone can greatly increase the catalytic activity. Another experiment was carried out to demonstrate that even at a constant temperature, the Seebeck voltage alone can increase the reaction rate substantially. BCSO powders were mixed with Pt containing solvent H_2PtCl_6 to form a green ceramic and it was sintered at 823 K for 1h before being used as a catalyst for this investigation (sample Pt(NP)/BCSO). This sintering temperature was 100 K lower, and the duration was only a tenth of the usual used (923K for 10hrs) for other samples, so this ceramic was not fully sintered. As a consequence, the BCSO can continue its crystallization processes in the reaction chamber with time, and therefore change its TE properties such as the Seebeck coefficient. **Figure 3a** shows XRD patterns for the back side and the front side of the Pt(NP)/BCSO after the catalytic reaction experiment. The back side's temperature never exceeded 350 K, so no further sintering could take place and it maintained the structure of the as-prepared green ceramics, which contained some 2nd phases such as Bi_2O_3. The hot side experienced temperatures of up to 773 K for several hours, allowing further crystallisation and sintering in the reaction chamber which reduced the amount of the second phase materials and increased its crystallinity, as indicated by Figure 3a.

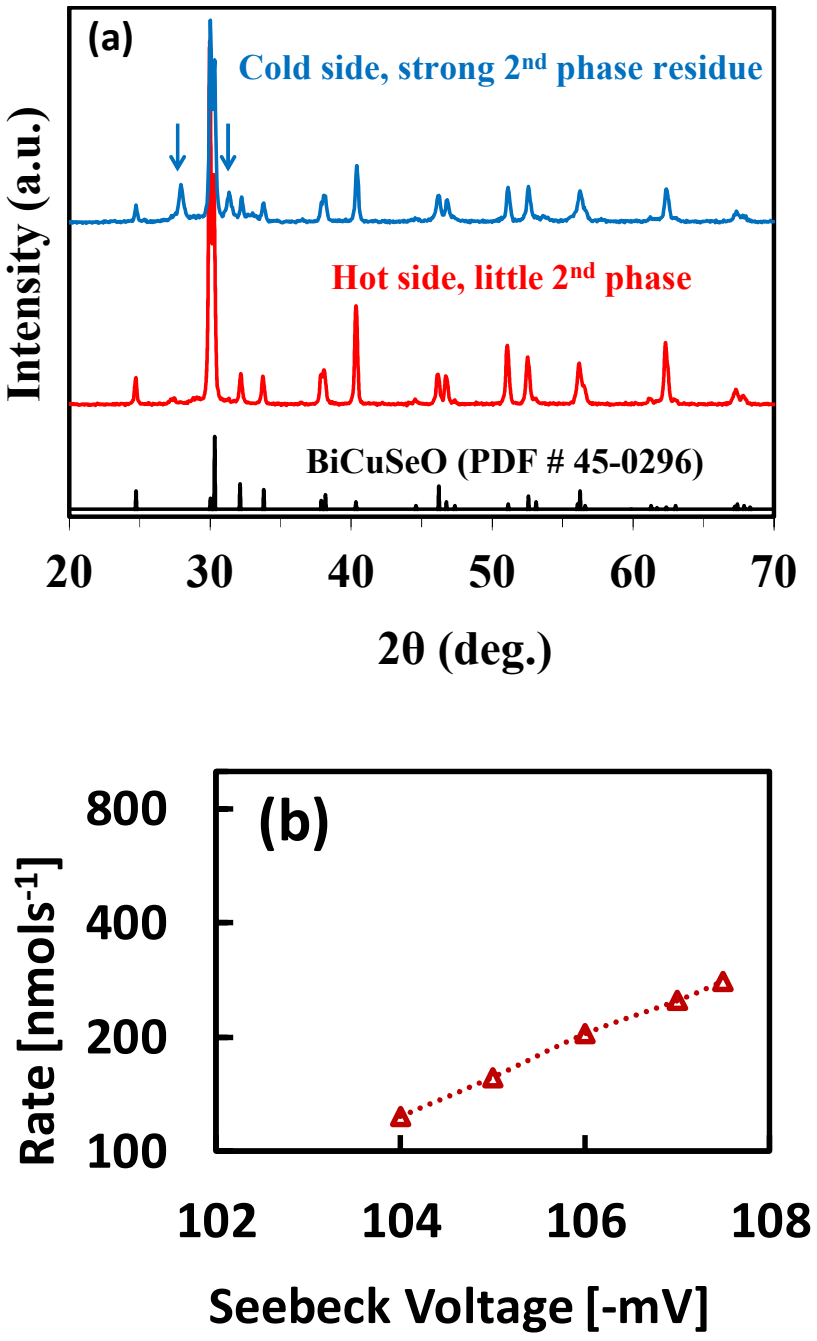

Figure 3. (a) XRD patterns for the cold side (top) and the hot side (bottom) of the Pt(NP)/BCSO after catalytic reaction measurement. (b) The ethylene oxidation rate as a function of the Seebeck voltage at constant temperatures T_h= 705 K and T_c= 339 K for Pt(NP)/BCSO. The increase in the Seebeck voltage was due to the increase of its Seebeck coefficient. Notice the logarithm scale for rate.

The effect of the increased Seebeck voltage on the reaction rate was monitored as a function of time while the chamber temperature was kept the same. **Table S3** summarises the reaction rates at different Seebeck voltages at a constant T_c and T_h, so therefore the rate increase can be attributed to the change of the Seebeck voltage. An excellent exponential increase of the reaction rate with the Seebeck voltage was observed (**Figure 3b**), demonstrating that the change of the Seebeck voltage alone can increase the catalytic reaction rate significantly.

Relationships between Seebeck voltage and catalytic activity. Figure 4 shows the relationships for the temperature, Seebeck voltage, and catalytic reaction rate for ethylene oxidation for the three samples; Pt(80)/$BCSO_{0.9}YSZ_{0.1}$, Pt(15)/BCSO, and BCSO only (without any Pt). **Figure 4a** shows their temperature dependence on the reaction rate. All three samples, show a similar behaviour to the sample Pt(80)/BCSO TE, i.e. an increase of 3 to 4 orders of reaction rate and 100% C_2H_4 conversion (**Figure S3**) when the temperature was increased from 300 K to around 700 K. This showed BCSO, like other conductive oxides such as IrO_2 and RuO_2, have high catalytic activity for ethylene oxidation. [26] The Seebeck voltage was recorded continuously during the experiment, and a typical time profile of the Seebeck voltage, for the sample BCSO, is shown in **Figure S4**. The Seebeck voltages at different temperature differences ΔT for all four samples are shown in **Figure 4b**. The negative voltage means the potential was lower at the hot surface T_h than at the cold surface T_c. All the Seebeck voltages were zero at room temperature, and increased linearly with ΔT. The extracted best-fit line gradients, i.e. the Seebeck coefficients, were different for different samples, and ranged from 206 μV/K for Pt(80)/$BCSO_{0.9}YSZ_{0.1}$ to 485 μV/K for BCSO. These Seebeck coefficients for BCSO

were within the values for BCSO reported in literature.[17-19] For the same temperature, the measured Seebeck voltage was higher for Pt(15)/BCSO and BCSO, than for the composite Pt(80)/$BCSO_{0.9}YSZ_{0.1}$. It was expected the composite sample to have a lower Seebeck coefficient, since YSZ was not a TE material. For all these four samples, the Seebeck coefficients decreased at high temperatures. This is not unusual, as generally speaking, the Seebeck coefficient of a TE material is temperature dependent.

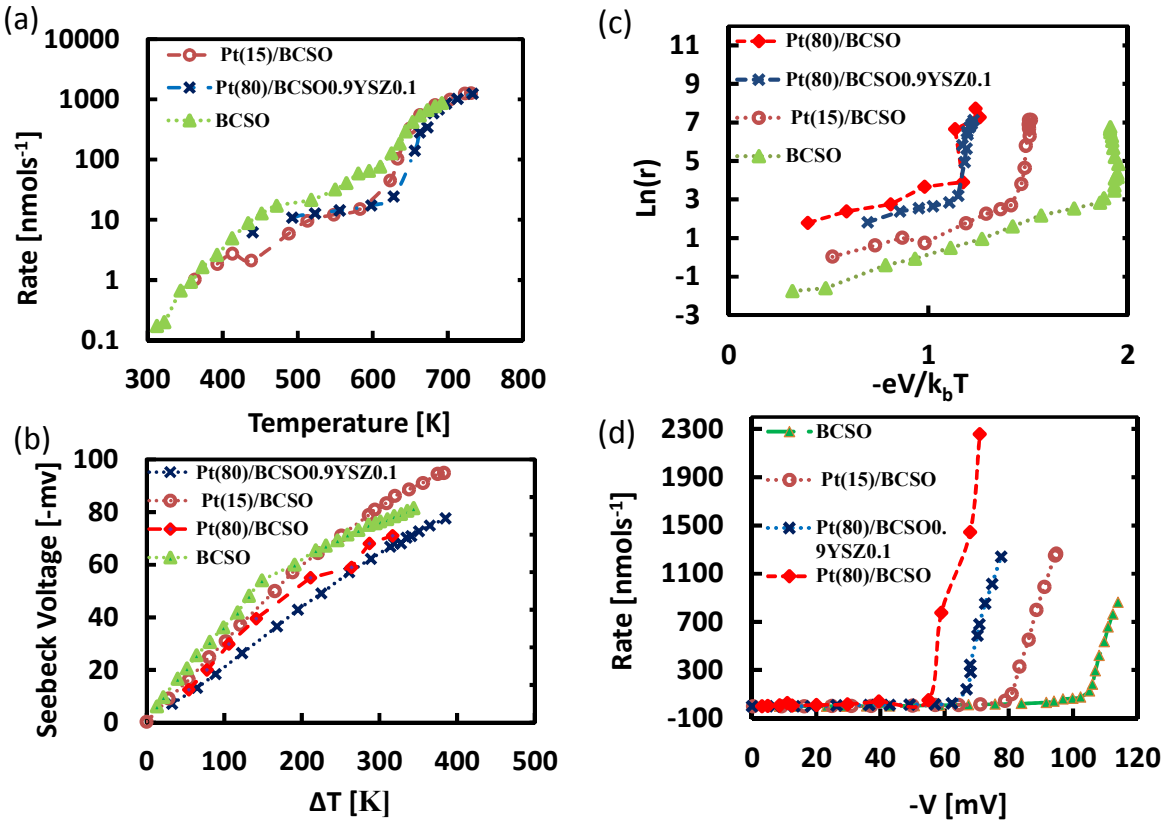

Figure 4. (**a**) reaction rate r increased by more than 3 orders with the increase of the temperature T_h. (**b)** measured Seebeck voltages as functions of temperature gradient across sample thickness. (**c)** a linear relationship between Ln(r) and -eV/k_bT_h when the Seebeck voltage was small. (**d)** at higher T_h with large Seebeck voltages, the rate r was proportional to the Seebeck voltage V.

In the following analysis, we assume the intrinsic ethylene oxidation was the rate limiting step. More precisely, under the fuel-lean conditions explored in this study, the rate-limiting step has been suggested to be the reaction between ethylene and adsorbed oxygen atom at the catalyst surface. [23] We further assume there were no mass transportation limitations (as discussed later this was only the case when the reaction rate was smaller than a certain value). There were several reasons to justify this assumption. As shown in Figure 1, there should be no pore-diffusion limitation as the samples were not porous. Also, a large temperature difference (~200-300 K when T_h >500 K) existed between the hot-surface T_h and the bottom of the chamber (see Figure S1a and Figure S2), there should be strong gas convection within the chamber, especially in a perpendicular direction. This can increase the reactants supply to the T_h surface and take away the reaction products. Also, it is known that CO_2 is a very stable chemical and the reaction of CO_2 with H_2O under excess oxygen environment is very difficult to take place. [24] Furthermore, the absolute concentrations of the reactants were relatively small, the initial partial pressures for C_2H_4 and O_2 were 0.189 kPa and 3.01 kPa, respectively. For these reasons, the ethylene oxidation was considered irreversible. The fact that all four experiments achieved 100% conversion of ethylene at about 700 K (Figure S3) provided further support for these assumptions.

In principle, the ethylene oxidation could have been carried out on the front surface (nominal surface area 314 mm^2) T_h, and back surface T_c, as well as the side wall of the disc samples. All our measurement data, (Table S1), showed no observable reaction rate for T_h < 350 K. At the same time, T_c was always below this temperature, so the rate contribution from the T_c surface (nominal surface area 314 mm^2) was

negligible for all samples under the TE conditions. We further assumed that the rate contribution from the side wall (with nominal area 126 mm^2) was also negligible (will be discussed later), and therefore the measured ethylene oxidation rate was attributed to the hot surface T_h only. **Figure 4c** shows the plotted data of Ln(r) versus $-eV/k_bT_h$ for all four samples. It can be seen for each sample, that under a certain temperature or Seebeck voltage, a linear relationship existed between Ln(r) the logarithm of the reaction rate, and $-eV/k_bT_h$ the ratio between the Seebeck energy and the thermal energy, the same as those observed for CO_2 hydrogenation.[14] The best-fit line gradients γ were 2.8, 2.4, 3.0, and 3.2 for Pt(80)/BCSO, Pt(80)/$BCSO_{0.9}YSZ_{0.1}$, Pt(15)/BCSO, and BCSO, respectively. For p-type TE materials, V is negative, from the equation $Ln(r/r_0) = -\gamma eV/k_bT_h$ it can be seen that the reaction rate should be much higher with a TE voltage than without. Looking at the data for Pt(80)/BCSO (Table S1) when T_h = 543 K; $Ln(r/r_0)$ = 3.29, so r/r_0 =26.8. This means at the temperature 543 K, the reaction rate was promoted by 26.8 times with a Seebeck voltage of -55 mV.

The ethylene oxidation also depends on the pre-exponential term, such as the total surface area and adsorptions. These factors may account for the rate dependence on sample materials in Figure 4a & c. Two reasons contributed to the observed result that the bare BCSO has similar ethylene oxidation rate as the Pt covered Pt(80)/BCSO: the exponential term with a high Seebeck voltage was the dominant factor and oxygen is adsorbed to the negatively charged surfaces of Pt and BCSO.

Catalytic activity with a high Seebeck voltage. Referring to Figure 4c again, no linear relationship was observed between Ln(r) and $-eV/k_bT_h$ with further increasing of the temperature and Seebeck voltage. For all of the samples, at high temperatures, Ln(r) increased rapidly whilst $-eV/k_bT_h$ changed little, or even reduced

for BCSO. In fact a good linear relationship between the rate r and the Seebeck voltage V was observed (**Figure 4d**). The parameter conditions at which the rate started to increase linearly with V (i.e. temperature, Seebeck voltage, $-eV/k_bT_h$, Ln(r)) were as follows: (543 K, -55 mV, 1.18, 4.94) for Pt(80)/BCSO, (656 K, -69 mV, 1.18, 4.94) for Pt(80)/$BCSO_{0.9}YSZ_{0.1}$, (633 K, -81 mV, 1.48, 4.63) for Pt(15)/BCSO, and (625 K, -105.2 mV, 1.95, 4.85) for BCSO. For all of the four samples, these "transition points" had very similar Ln(r) values, 4.94, 4.94, 4.63 and 4.85 respectively, suggesting the reaction rate was the main factor determining the "transition point". The extracted line gradients for the four samples were similar, and were 122.4, 101.9, 82.6 and 85.5 nmol mV^{-1} respectively.

Figures 4c-d show that once the reaction rate reached above 120 $nmols^{-1}$, the relationship between the reaction rate r and the Seebeck voltage V changed from exponential to linear. We believe this was due to the change of the rate limiting mechanism. At low reaction rate (<120 $nmols^{-1}$), the ethylene oxidation was activation energy limited. However, at higher rate >140 $nmols^{-1}$, the ethylene oxidation became either mass transfer limited or charge transfer limited. If it was charge transfer limited, one would expect different materials (BCSO, Pt(80)/BCSO or Pt(15)/BCSO) to have different "transition point" because their surface electrical conductivity should be different. The fact that all the different samples had the "transition point" at the same reaction rate suggested that the mass transfer of reactant, most likely to be ethylene transfer (as the inlet gases were highly oxygen rich) was the rate limiting step. The gradients for different samples as shown in figure 4d had similar values, further supporting the assumption that the rate limiting factor was the ethylene mass transport, independent of the catalyst samples. Both the Seebeck voltage and the ethylene diffusion (onto the reaction surface) were

proportional to the temperature gradient, which resulted in an apparent linear relationship between the reaction rate and the Seebeck voltage.

It is interesting to notice that the r — (-V) curves as shown in figure 4c-d resemble the I — V curve for a p-n diode under bias, where an I-V linear relationship at high voltage is often observed. [27] The “transition point” in figure 4c-d is analogous to the “knee point” in the I—V curve of a p-n junction. This is not entirely surprising as there is similarity between the Schottky barrier formed at the Pt-BCSO interface and a p-n junction in a diode (this will be discussed later).

Under TE conditions, the T_c side never reached more than 350K, and no reaction was ever recorded for T_h less than 350K, therefore it was a fact that no reaction had taken place on the T_c side under TE conditions. Under RTE conditions, the T_c side could have reached temperatures higher than 350K, however, the Seebeck voltage at the T_c side was positive, so the rate equation on the T_c side becomes $Ln(r/r_0) = -\gamma eV/k_bT_c < 0$ because $V > 0$. This means the reaction rate on the T_c side was effectively inhibited, and the rate on the T_c side should be much smaller than the rate at the T_h side under RTE conditions. For the same reason, as the temperature at the side wall was always lower than at the hot surface, due to the thermoelectric promotion of catalysis, the reaction rates at the side wall were negligible relative to that on the T_h side.

Having established the reactions were mainly taking place on the T_h surface, the turnover frequency (TOF) can be estimated. For simplicity we consider Pt(80)/BCSO where the surface was a continuous Pt layer, with a nominal area 314 mm^2. The actual surface area should be larger (but less than twice if not porous and using sphere particle model) due to the surface roughness, but usually not all the surface

area is catalytically active. Taking all these into consideration we use the nominal area as the total surface area. Pt is cubic with a lattice constant 0.3924 nm. So there are $2x10^{15}$ surface Pt atoms on the T_h side. For a rate of 120 $nmols^{-1}$, the corresponding TOF was 36 s^{-1}.

Electron Fermi levels change with temperature. Combining the previously reported results,[14] the TEPOC phenomena has been demonstrated on two different chemical reactions, namely CO_2 hydrogenation and ethylene oxidation. Also, it was reported recently that thermoelectric materials can function as electrocatalysts and Seebeck voltage can initiate and boost electrocatalytic reactions. [28] We believe the mechanisms for all these were the same and will be discussed below. With the help of numerical modelling, we show that the electrochemical energy of electrons in the TE material increases with temperature, as a result, its work function and those for the Pt supported on it were decreased.

The platinum supported on BCSO (Pt/BCSO) is a typical metal on semiconductor system. According to metal-semiconductor contact theory, the Fermi levels of the metal and the semiconductor should be the same at the surface after the contact. Before contact, the metal and the semiconductor have different work functions, and then upon contact, charge will flow to the material with a lower Fermi level, until their Fermi levels are equalized.[29,30]

The work function and Fermi level of BCSO and their temperature dependence were calculated using *ab initio* method based on density functional theory.[31,32] **Figure 5** shows (a) the electrostatic potential distribution, and (b) charge density difference at the interface for the optimised structure of eight layers of Pt on two unit cells of BCSO along the [001] direction at the room temperature. In **Figure 5b**, yellow and

blue represent gaining and losing of electrons respectively, it can be seen that charge transfer happened mainly from Bi to Pt. From the first principle calculation, the obtained work functions were 3.94 eV for the intrinsic BCSO, and 5.67 eV for Pt which is close to its experimental value 5.64 eV.[33] As BCSO has a much smaller work function than Pt, upon contact electrons will be transferred from BCSO to Pt, forming a Schottky barrier at the interface.

The Fermi level of BCSO changes with temperature as well, **Figure 6** shows the calculated Fermi levels of BCSO as functions of temperature at different charge carrier concentrations. At a particular temperature, higher carrier density leads to a smaller change in the Fermi level. At a particular charge carrier density, higher temperature makes the Fermi level move closer to the intrinsic value (middle of the band gap). For the p-type BCSO, the Fermi level increases with increasing temperature, and for a n-type BCSO, its Fermi level decreases with increasing temperature.

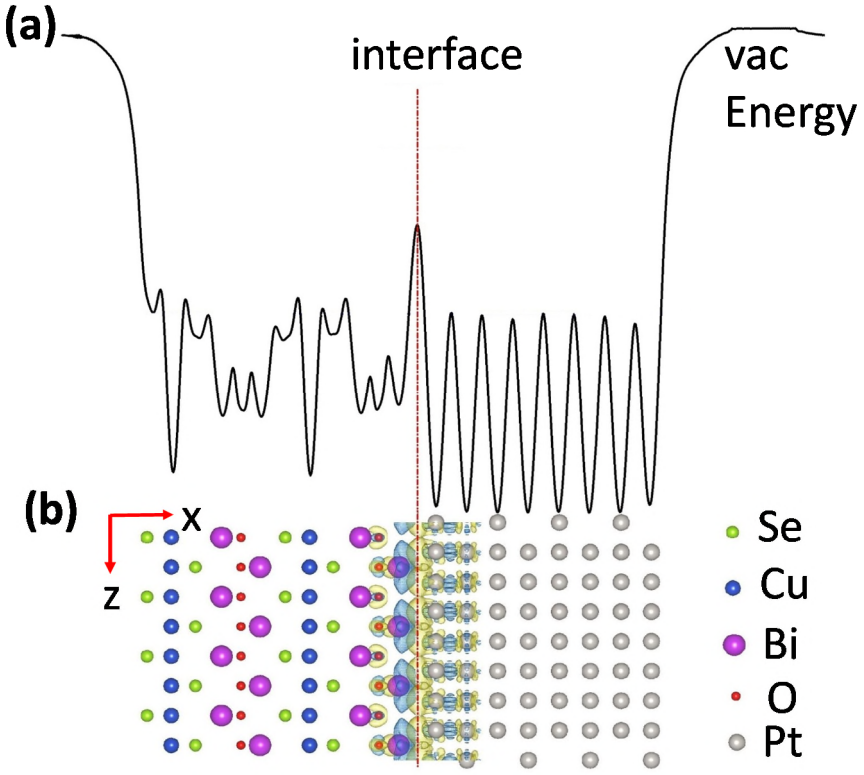

Figure 5. (**a)** the distribution of electrostatic potential; (**b)** the charge density difference.

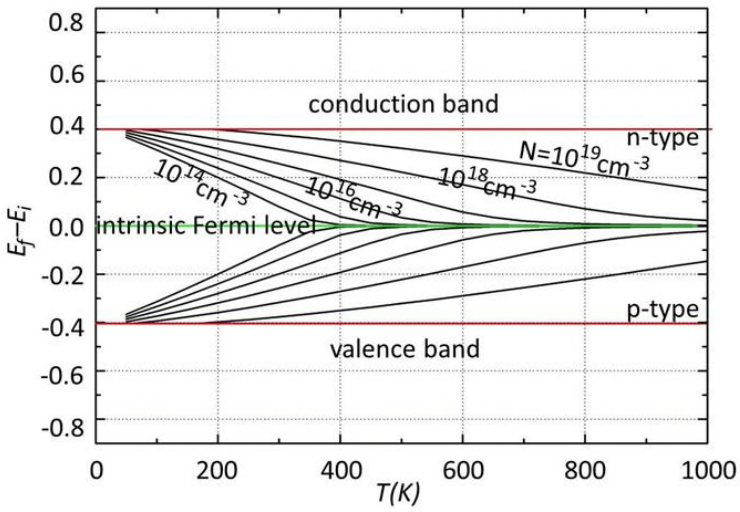

Figure 6. The Fermi level dependence on temperature at different charge carrier concentrations for n-type and p-type BCSO.

Electron work function changes with the Seebeck voltage. Work function is defined as the minimum energy required to remove an electron from a material to vacuum immediately outside its surface. It is a measure of how tightly a material holds its electrons, and can affect many of the material's properties especially the surface and interfacial properties. [34-36] In general, work function is determined by the electrochemical energy (Fermi level) ε_F and the inner potential χ, i.e.

$$\varphi = -\varepsilon_F - e\chi \qquad (2)$$

According to definition a voltmeter measures the difference in electrochemical energy, which equals the Seebeck voltage V,

$$-eV = \varepsilon_{F,h} - \varepsilon_{F,c} = -(\varphi_h - \varphi_c) - e(\chi_h - \chi_c) = -\Delta\varphi - e(\chi_h - \chi_c) \qquad (3)$$

here the subscripts h and c indicates hot and cold sides respectively.

$$\text{Or } \Delta\varphi = eV - e\Delta\chi \qquad (4)$$

In other words, the change of work function is consisted of two parts, one from the change of the Femi level which equals to eV for TE materials, and the other from the change of the inner potential.

Generally speaking the electron work function for metals decreases with increasing temperature, with a linear coefficient about $-(1\sim15)\times10^{-5}$ eVK^{-1}.[37] This can be understood by regarding the work function as a barrier for the electrons to be moved from inside a solid to a point in vacuum immediately outside the solid surface.[34] Increasing temperature should thermally excite electrons to be able to move out easier. As a rough estimation, in metals the reduction in work function was assumed equal to the thermal energy of an electron $\frac{3}{2}k_bT$: [38,34]

If we apply the above estimation to the oxide BCSO as well, i.e., the reduction in work function for the non-thermoelectric origin equals to $\beta k_b \Delta T$ where β is a constant, then for thermoelectric materials we have

$$\Delta \varphi = -eS(T_h - T_c) - \beta k_b(T_h - T_0) \qquad (5),$$

if the cold side temperature T_c is not the same as the initial temperature T_0.

So the change of work function is linearly proportional to the temperature gradient, and, when the magnitude of the Seebeck coefficient $|S| \gg \beta k_b/e$, it is equal to eV. As it has been established that the work function change at catalyst's surface will lead to the exponential change of the reaction rate, [22] the experimentally observed equation $\mathrm{Ln}(r/r_0) = -\gamma eV/k_bT$ can therefore be explained. It should be emphasised here it is the change of Work Function, not the Fermi level, that is responsible for the change of the reaction rate. This has been well discussed in the case for NEMCA.[39]

Charge transfers accompanying the temperature change. For Pt supported on the p-type BCSO, upon a temperature increase, the Fermi level of the BCSO increases, but Pt's Fermi level hardly changes, and as a consequence more electrons are transferred from BCSO to Pt, reducing the work function of the Pt further.

So the change of the work function for Pt supported on BCSO has two aspects. The first is the reduction of work function due to the difference in their work functions upon contact. The second aspect is the further reduction of work function with the increasing temperature due to the TE effect, as discussed above.

It can be shown there is a net charge built up on the surface of a thermoelectric material with the increase of temperature. This is similar to the case of the Pt

supported on BCSO, which could at least partially explain the observed similar catalytic behaviours as shown in Figure 4. Take an example of a p-type TE disc of 20 mm in diameter and thickness L, with its cold side at T_c and hot side at T_h, and Seebeck coefficient S. The total Seebeck voltage is $V_0 = -S(T_h-T_c)$. If Z axis is along the thickness direction, with origin at the cold side, at any point z within TE, $V(z) = V_0z/L$ assuming the temperature gradient within TE is uniform. From Poisson's equation, we know the free charge density within TE is zero, and electrical field $E = V_0/L$ is a constant. The surface charge density is $\sigma = \varepsilon_0\varepsilon E = \varepsilon_0\varepsilon V_0/L$, where ε_0 is the dielectric constant of vacuum, and ε the relative permittivity of the TE material. So at the hot surface, the net charge density is $\sigma_h = -\varepsilon_0\varepsilon S(T_h-T_c)/L$, and at the cold surface, the net charge density is $\sigma_c = \varepsilon_0\varepsilon S(T_h-T_c)/L$. Take the values of $T_h-T_c = 300K$, $S = 300\ \mu VK^{-1}$, $\varepsilon = 5$ (calculated relative permittivity for BCSO), L=2 mm, then $\sigma_h = -2 \times 10^{-9}\ Cm^{-2}$, or $\sim 1.25 \times 10^6$ electrons per square centimetre. This is a small charge density. Nevertheless, this net surface charge and surface potential should have a significant effect on the surface, for example the adsorption property. This suggests that the reduced work function, and the negative charges on the surface, will reduce the activation energy for the reaction between the ethylene and the adsorbed oxygen atom, therefore makes the whole reaction easier. Further studies are needed to reveal the specific mechanisms for thermoelectric promotion of catalysis of a particular reaction.

TEPOC is an universal phenomenon. Generally chemical reactions follow the Arrhenius law (**Figure S5**), i.e. $r_0 = k_0 \exp(-E_a/k_bT)$, here E_a is the activation energy of the reaction, and k_0 a constant. Combining Equation (1) with Arrhenius law gives $r = k_0 \exp(-(E_a + \gamma eV)/k_bT)$, hence the activation energy is reduced by $-\gamma eV$ (a negative number for the cases here).

Apparently there are similarities and differences between TEPOC and NEMCA. Both achieve the promotion of catalysis through a change of electron work function of the catalyst surface, but the mechanisms to achieve the change of work function are different. In TEPOC, the change of work function is mainly due to the change of Fermi level, a direct electronic effect of thermoelectricity. Whilst in NEMCA it is the formation of a double-layer leads to the change of work function. NEMCA has been observed in over 80 different chemical reactions.[4, 5, 10-11] The similarity in the underlying fundamental mechanisms between the two make us believe TEPOC can also be observed in those reactions.

A major difference is that a solid state electrolyte is a critical component in NEMCA but it is not needed in TEPOC. It has been reported that BCSO has negligible ionic conductivity,[40,41] i.e. any spillover of ionic species was negligible. Also, we did observe the NEMCA phenomenon for the Pt(80)/YSZ (**Figures S5-S7**). However, when a positive or negative voltage was applied onto the Pt(80)/BCSO or Pt(80)/$BCSO_{0.9}YSZ_{0.1}$ using a typical NEMCA configuration, no noticeable change of reaction rate could be observed. This is understandable because TE materials are electrically conductive, a non-ohmic potential drop could not be realised through an external applied voltage across this material.

▪ CONCLUSIONS

In summary, we have investigated an innovative use of the thermoelectric ceramics as a catalyst support and promoter, through the ethylene C_2H_4 oxidation to produce CO_2 and H_2O. It was found that the catalytic activity of Pt supported on the thermoelectric materials can be promoted significantly by a Seebeck voltage, which

was produced directly by a temperature difference across its thickness. Also, the thermoelectric material BiCuSeO itself was found to be catalytically active for ethylene oxidation, and it can also be promoted significantly by a Seebeck voltage. Furthermore, catalytic activity was found to increase exponentially with $-eV/k_bT$ when the reaction was activation energy limited. However, upon further increase of the reaction rate, the process became mass transport limited and instead, a linear relationship between the reaction rate and the Seebeck voltage was observed. Further analysis indicates that this thermoelectric promotion of catalysis was accompanied by a charge transfer from the thermoelectric material to the metal catalyst on the surface or from the bulk to the surface thermoelectric materials, and the thermoelectric promotion of catalysis was due to the change of the catalyst work function with temperature and temperature gradient of the thermoelectric materials.

- ASSOCIATED CONTENT

  The Supporting Information is available free of charge on the ACS Publications website.

  Detailed summary of experimental conditions and measurement results for Figure 2 and Figure 3, Schematic of the reaction chamber and the experimental set-up, and the measurement parameters, Temperature dependence of the C_2H_4 conversion for the corresponding four samples in Figure 2 and Figure 4, Detailed time profile of the recorded Seebeck voltage during the experiment for the BCSO in Figure 4, Arrhenius plot for the ethylene oxidation on Pt(80)/YSZ, and the SEM images, Schematic of the set-up and measurement results for Non-Faradaic-electrochemical-modification-of-catalytic-activity (NEMCA) characterisation for Pt(80)/YSZ, Ab initio simulation and modelling.

▪ AUTHOR INFORMATION

*Corresponding author e-mail: Z.Huang@cranfield.ac.uk

ORCID: 0000-0002-7195-3189

▪ **ACKNOWLEDGMENTS**

The work was financially supported by a Leverhulme Trust Research Project Grant (RPG-2013-292), and a Joint Research Fund of NSFC (No. 51428101) for Hong Kong and Macao and Overseas Scholars. We thank Mr. A. Stallard, T. Pryor, and X. Liu of Cranfield University for technical help. ZH is grateful to Profs. R. Whatmore of Imperial College London, Chris Hardacre of the University of Manchester, Gao Min of Cardiff University and Antonio De Lucas Consuegra of Universidad de Castilla-La Mancha of Spain for invaluable discussions.

▪ **REFERENCES**

(1) Gänzler, A. M.; Casapu, M.; Vernoux, P.; Loridant, S.; Cadete Santos Aires, F. J.; Epicier, T.; Betz, B.; Hoyer, R.; Grunwaldt, J.-D., Tuning the Structure of Platinum Particles on Ceria In Situ for Enhancing the Catalytic Performance of Exhaust Gas Catalysts, *Angew. Chem. Int. Ed*., **2017**, 56, 13078-13082.

(2) Kalz, K. F.; Kraehnert, R.; Dvoyashkin, M.; Dittmeyer, R.; Gläser, R.; Krewer, U.; Reuter, K.; Grunwaldt, J.-D., Future Challenges in Heterogeneous Catalysis: Understanding Catalysts under Dynamic Reaction Conditions, *ChemCatChem.*, **2017**, 9, 17–29.

(3) Chen, W.; Wang, H.; Li, Y.; Liu, Y.; Sun, J.; Lee, S.; Lee, J.; and Cui, Y., In Situ Electrochemical Oxidation Tuning of Transition Metal Disulfides to Oxides for Enhanced Water Oxidation, *ACS Cent. Sci.*, **2015**, 1, 244-251.

(4) Vayenas C.G.; Bebelis, S.; Pliangos, C.; Brosda, S. and Tsiplakides, D., *Electrochemical Activation of Catalysis: Promotion, Electrochemical Promotion, and Metal-Support Interactions*, Kluwer Academic/Plenum Publishers, New York **2001**.

(5) Vayenas, C.G.; Brosda, S.; and Pliangos, C., The Double-Layer Approach To Promotion, Electrocatalysis, Electrochemical Promotion, And Metal-Support Interactions, *J. Catal.,* **2003**, *216*, 487-504.

(6) Poulidi, D.; Anderson, C. and Metcalfe, I., Remote Control Of The Activity Of A Pt Catalyst Supported On A Mixed Ionic Electronic Conducting Membrane, *Solid State Ionics*, **2008**, *179*, 1347-1350.

(7) Konsolakis, M.; Macleod, N.; Isaac, J.; Yentekakis, I. and Lambert, R., Strong Promotion By Na Of Pt/Γ-Al_2O_3 Catalysts Operated Under Simulated Exhaust Conditions, *J. Catal.,* **2000**, *193*, 330-337.

(8) Lucas-Consuegra, A.; González-Cobos, J.; García-Rodríguez, Y.; Endrino, J.L.; Valverde, J.L., Electrochemical Activation Of The Catalytic Methanol Reforming Reaction For H_2 Production, *Electrochemistry Commun.*, **2012**, *19*, 55-58.

(9) Harkness, I. R.; Hardacre, C.; Lambert, R. M.; Yentekakis, I. V.; Vayenas, C. G., Ethylene Oxidation Over Platinum: In Situ Electrochemically Controlled Promotion Using Na-B″ Alumina And Studies With A Pt(111)/Na Model Catalyst, *J. Catal.* 1996, ***160***, *19-26*.

(10) Tsiplakides, D. and Balomenou, S., Electrochemical Promoted Catalysis: Towards Practical Utilization, *Chem. Indust. & Chem. Eng. Quart*., **2008**, *14*, 97-105.

(11) Kambolis, A.; Lizarraga, L.; Tsampas, M.; Burel, L.; Rieu, M.; Viricelle, J;, Vernoux, P., Electrochemical promotion of catalysis with highly dispersed Pt nanoparticles, *Electrochemistry Commun*., **2012**, *19*, 5-8.

(12) Wang, Z.; Huang, H.; Liu, H.; Zhou, X., Self-Sustained Electrochemical Promotion Catalysts For Partial Oxidation Reforming Of Heavy Hydrocarbons, *Inter. J. Hydro. Energy*, **2012**, 37,17928-17935.

(13) Pramuanjaroenkij, A.; Zhou, X.; Kakac, S., Numerical Analysis Of Indirect Internal Reforming With Self-Sustained Electrochemical Promotion Catalysts, *Inter. J. Hydro. Ene.,***2012**, 35, 6482-6489.

(14) Achour, A.; Chen, K.; Reece, M. and Huang, Z., Tuning Of Catalytic Activity By Thermoelectric Materials For Carbon Dioxide Hydrogenation, *Adv. Energy Mater.*, **2018**, 8, 1701430.

(15) Ohta, H.; Sugiura, K. and Koumoto, K., Recent Progress In Oxide Thermoelectric Materials: P-Type $Ca_3Co_4O_9$ And N-Type $SrTiO_3$, *Inorg. Chem.*, **2008**, 47, 8429-8436.

(16) He, J.; Liu, Y. and Funahashi, R., Oxide Thermoelectrics: The Challenges, Progress, And Outlook, *J. Mater. Res*., **2011**, 26, 1762-1772.

(17) Barreteau, C.; Pan, L.; Amzallag, E.; Zhao, L. D.; Berardan, D.; Dragoe, N., Layered Oxychalcogenide In The Bi–Cu–O–Se System As Good Thermoelectric Materials, *Semicond. Sci. Technol.,* **2014***,* 29**,** 064001.

(18) Barreteau, C., Berardan, D., Dragoe, N., Studies On The Thermal Stability Of Bicuseo, *J. Solid State Chem.* **2015**, 222, 53-59.

(19) Zhao, L.D.; He, J.; Berardan, D.; Lin; Y., Li, J.; Nan, C. and Dragoe, N., Bicuseo Oxyselenides: New Promising Thermoelectric Materials, *Energy and Environ. Sci.,* **2014***,* 7, 2900-2924;

(20) Li, F.; Wei, T.; Kang, F.; and Li, J., Thermal Stability And Oxidation Resistance Of Bicuseo Based Thermoelectric Ceramics, *J of Alloys and Compounds*, **2014**, 614, 394-400.

(21) Wunderlich, W.; Mori, T. and Sologub, O., SPS-Sintered $NaTaO_3$-Fe_2O_3 Composite Exhibits Large Seebeck Coefficient And Electric Current, *Mater. Renew. Sustain. Energy,* **2014**, 3, 21-25.

(22) Vayenas, C.G.; Bebelis, S. and Ladas, S., Dependence Of Catalytic Rates On Catalyst Work Function, *Nature*, **1990**, 343, 625-627.

(23) Bebelis, S. and Vayenas, C.G., Non-Faradaic Electrochemical Modification of Catalytic Activity 1. The Case of Ethylene Oxidation on Pt, *J. of. Catal*., **1989**, 118, 125-146.

(24) Wang, W.; Wang, S.; Ma, X. and Gong, J., Recent Advances In Catalytic Hydrogenation Of Carbon Dioxide, *Chem. Soc. Rev.*, **2011**, 40, 3703-3727.

(25) Achour, A.; Chen, K.; Reece, M. and Huang, Z., Enhanced thermoelectric performance of Cs doped BiCuSeO prepared through eco-friendly flux synthesis, *J. Alloys & Comp.* **2018**, 735, 861-869.

(26) Nicole, J., Tsiplakides, D., Wodiunig, S., and Comninellis Ch., Activation Of Catalyst For Gas-Phase Combustion By Electrochemical Pretreatment, *J. Electrochem. Soc.***1997***,* 144, L312-314.

(27) Brophy, J. *Basic electronics for scientists*, McGraw-Hill, New York, **1990**.

(28) Sharifi, T.; Zhang, X.; Costin, G.; Yazdi, S.; Woellner, C.; Liu, Y.; Tiwary, C. and Ajayan, P., Thermoelectricity Enhanced Electrocatalysis, *Nano Lett.*, **2017**, 17, 7908-7913.

(29) Ioannides, T. and Verykios, X.,Charge Transfer in Metal Catalysts Supported on Doped TiO_2: A Theoretical Approach Based on Metal-Semiconductor Contact Theory, *J. Catal.* **1996**, 161, 560-569.

(30) Zhang, Z. and Yates, J., Band Bending in Semiconductors: Chemical and Physical Consequences at Surfaces and Interfaces, *Chem. Rev.* **2012**, 112, 5520-5551.

(31) Kresse, G. and Furthmüller, J., Efficient Iterative Schemes For Ab Initio Total-Energy Calculations Using A Plane-Wave Basis Set, *Phys. Rev.,* **1996***,* B54, 11169-11186.

(32) Perdew, J.P.; Burke, K. and Ernzerhof, M., Generalized Gradient Approximation Made Simple*, Phys. Rev. Lett.* **1996**, 77, 3865-3868.

(33) Holzl, J. and Schulte, F.K. *Work Function of Metals, in Solid Surface Physics*, Springer-Verlag, Berlin, **1979**.

(34) Huang, X.; Yu, B.; Yan, X. and Li, D., Variations In Erosive Wear Of Metallic Materials With Temperature Via The Electron Work Function, *Mat. Chem & Phys*., **2016**, 172, 197-201;

(35) Rahemi, R. and Li, D., Variation In Electron Work Function With Temperature And Its Effect On The Young's Modulus Of Metals, *Scripta Mat.*, **2015**, 99, 41-44.

(36) Kaack, M. and Fick, D., Determination Of The Work Functions Of Pt(111) And Ir(111) Beyond 1100 K Surface Temperature *Surf. Sci.*, **1995**, 342, 111-118.

(37) Kiejna, A.; Wojciechowski, K. and Zebrowski, J., The Temperature Dependence Of Metal Work Functions, *J. Phys. F: Metal Phys.,***1979**, 9, 1361-1366.

(38) Dushman, S., Electron Emission From Metals As A Function Of Temperature, *Phys. Rev*., **1923**, 21, 623.

(39) Bebelis, S. and Vayenas, C.G., Non-Faradaic Electrochemical Modification of Catalytic Activity 5. Oxygen Chemisorption on Silver, *J. Catal*., **1992**, 138, 570-587.

(40) Vaqueiro, P.; Al Orabi, R.; Luu, S.; Guelou, G.; Powell, A.; Smith, R.; Song, J.; Wee, D.; and Fornari, M., The Role Of Copper In The Thermal Conductivity Of Thermoelectric Oxychalcogenides: Do Lone Pairs Matter?, *Phys. Chem. Chem. Phys.* **2015**, 40, 31735-31740;

(41) Zhao, L. and Li, J., *BiCuSeO: A promising thermoelectric material, in Materials Aspect of Thermoelectricity*, Uher, C., Editor, CRC Press, Boca Raton, USA, **2016**.

Supporting Information

In-Situ Tuning of Catalytic Activity by Thermoelectric Effect for Ethylene Oxidation

Abdenour Achour [+], Jian Liu [%], Ping Peng [%],

Christopher Shaw [+] and Zhaorong Huang [+*]

[+] Surface Engineering and Precision Institute, Cranfield University, Bedfordshire MK43 0AL, UK

[%] School of Materials Science & Engineering, Hunan University, Changsha 410082, China

*Corresponding author e-mail: Z.Huang@cranfield.ac.uk

Table S1: Summary of experimental conditions and catalytic reaction measurement results for Pt(80)/BCSO TE in Figure 2. T_c, T_h were the temperatures at the top (cold) and bottom (hot) surfaces respectively, V the Seebeck voltage.

Tc (K)	302.4	302.4	306.5	306.7	308.7	311.6	315.2	319.5	325.6	332.0	339.0	340.0	349.0
Th(K)	302.5	302.5	315	328.4	345	366	393	425.5	467	543	603	627	666
ΔT (Th-Tc)	0.1	0.1	8.9	21.7	36.3	54.4	77.8	106.0	141.4	211.0	264.0	287.0	317.0
Seebeck V (-mv)					7.9	12.5	20	29.8	39.5	55	59	68	71
CO_2 (kPa)	0.000	0.000	0.000	0.000	0.000	0.001	0.002	0.004	0.009	0.011	0.175	0.325	0.508
C_2H_4 (kPa)	0.194	0.195	0.197	0.196	0.195	0.194	0.194	0.192	0.187	0.165	0.015	0.001	0.000
O_2 (kPa)	2.99	2.94	2.91	2.85	2.85	2.85	2.85	2.85	2.83	2.84	2.66	2.42	2.23
r CO2 (nmol(O)/s)	0.0	0.0	0.0	0.0	0.0	6.0	10.9	15.7	38.9	49.8	775	1445	2258
C_2H_4 Conv (%)	0.0	0.0	0.0	0.0	0.0	0.3	0.6	0.9	2.3	3.3	84.9	99.1	99.9
ln (r)						1.78	2.39	2.75	3.66	3.91	6.65	7.28	7.72
$-eV/K_bT_h$						0.40	0.59	0.81	0.98	1.17	1.13	1.26	1.24

Table S2: Summary of experimental conditions and catalytic reaction measurement results for Pt(80)/BCSO RTE in Figure 2. T_h was the temperature at the bottom (hot) surface, V the Seebeck voltage. T_c was not measured, but could be calculated from the corresponding Seebeck voltage and the T_h.

T_h(K)	298	352	423	493	553	623	713	778
Seebeck V (-mv)				2.1	3.1	4.9	8.6	11
CO_2 (kPa)	0.0000	0.0000	0.0000	0.0000	0.0001	0.0020	0.0048	0.0178
C_2H_4 (kPa)	0.20	0.19	0.20	0.20	0.20	0.20	0.19	0.19
O_2 (kPa)	2.970	2.881	2.889	2.882	2.879	2.876	2.851	2.827
r CO2 (nmol(O)/s)	0.0	0.0	0.0	0.0	0.1	2.9	7.1	26.4
C_2H_4 Conv %	0.0	0.0	0.0	0.0	0.0	0.5	1.2	4.4
ln (r)					-2.5	1.1	2.0	3.3
$-eV/k_bT_h$				0.05	0.06	0.09	0.14	0.16

Table S3: Summary of Seebeck voltage, reaction rate and ethylene conversion at constant temperatures T_h = 705 K and T_c = 339 K for the sample Pt(NP)/BCSO in Figure 3.

V (-mV)	104	105	106	107	107.5
r_{CO2} (nmol (O)/s)	124	157	204	250	281
C_2H_4 Conv %	9.6	13.8	20.0	26.8	31.7

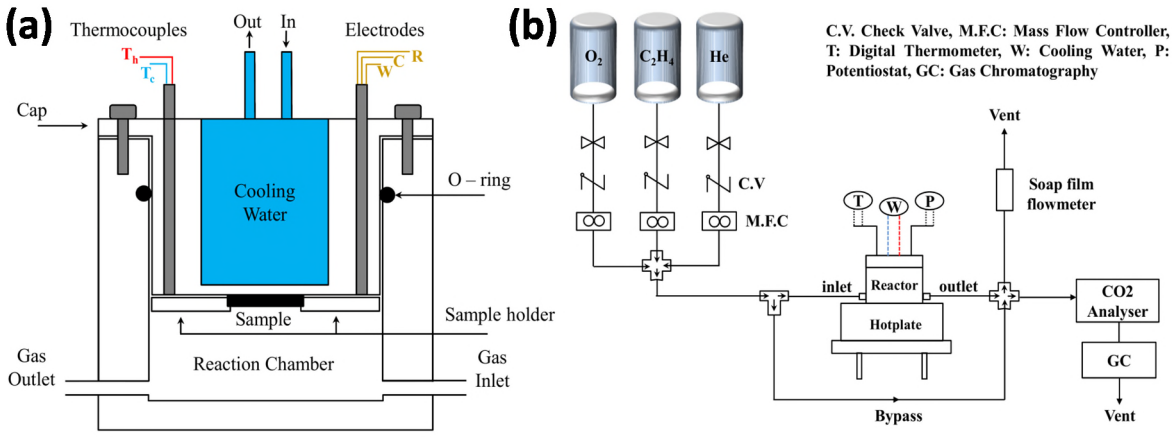

Figure S1. (a) Schematic of the single chamber reactor which can combine thermoelectric effect with catalytic chemical reaction. **(b)** Schematic of the experimental set-up for ethylene oxidation reaction characterisation.

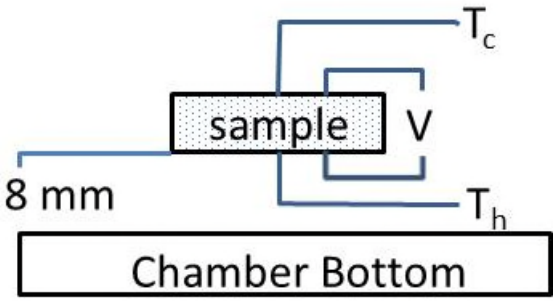

Figure S2. Schematic of the arrangement of the sample and the measurement parameters for all the catalytic reaction experiments. T_c and T_h were measured temperatures at the top and bottom surfaces of the sample, and V the corresponding Seebeck voltage. The bottom surface of the sample was about 8 mm above the bottom of the stainless steel chamber. The temperature of the chamber bottom was 200 ~ 300 K higher than the bottom of the disc sample.

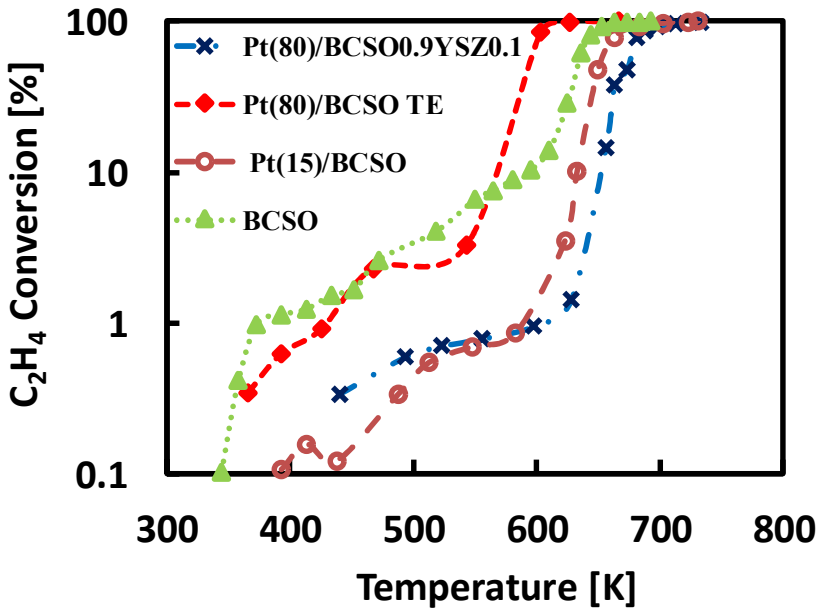

Figure S3. The corresponding ethylene conversions as functions of the temperature T_h for the Pt(80)/BCSO TE in Figure 2, and for the three samples BCSO, Pt(15)/BCSO, and Pt(80)/$BCSO_{0.9}YSZ_{0.1}$ in Figure 4a. The conversion was increased by 3 orders with the increase of the temperature T_h.

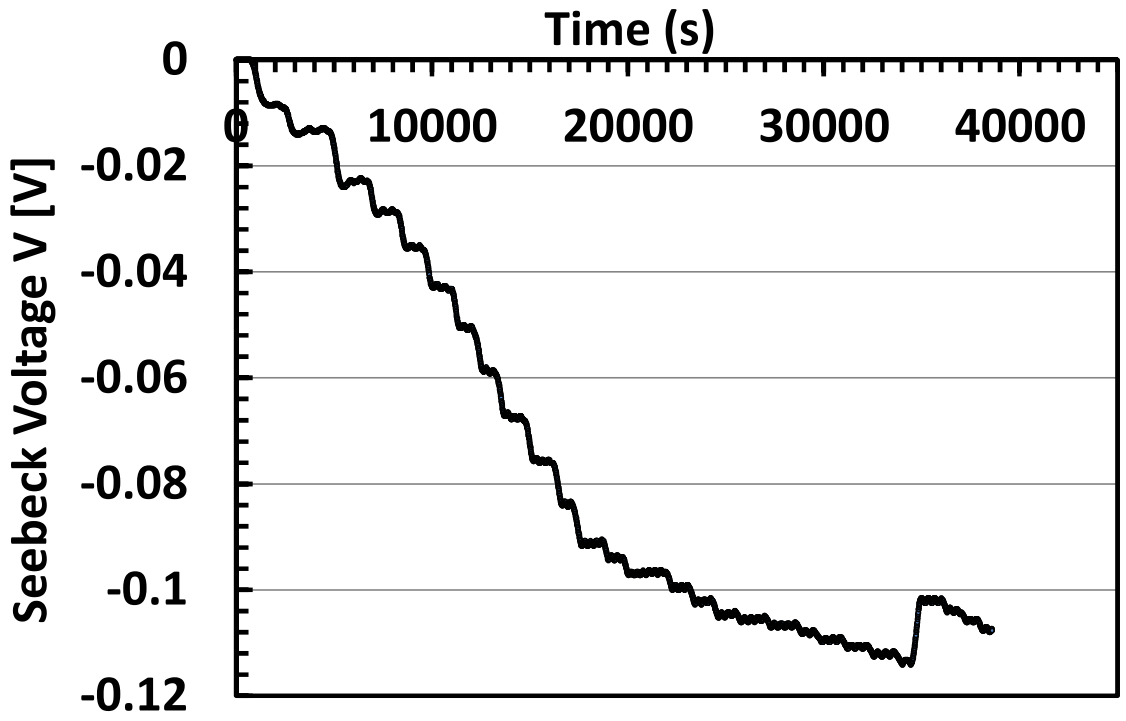

Figure S4. Time profile of the recorded Seekeck voltage during catalytic reaction characterisation experiment for the BCSO in Figure 4. Time zero was the start of heating up of the hot-plate. Gas concentration measurement using the gas chromatograph was carried out 30 minutes after a fixed Seebeck voltage is reached at a certain temperature. After that the temperature T_h was increased to the next value, which has a larger (more negative value) Seebeck voltage.

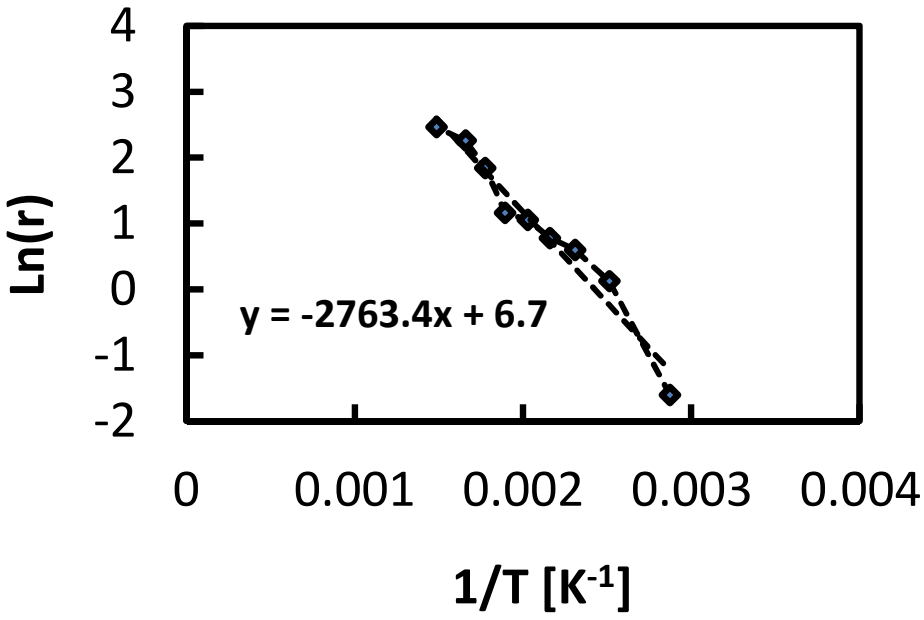

Figure S5. Arrhenius plot for the ethylene oxidation on Pt(80)/YSZ. Ln(r) as a function of 1/T for ethylene oxidation rate on Pt(80)/YSZ. YSZ is not a thermoelectric material.

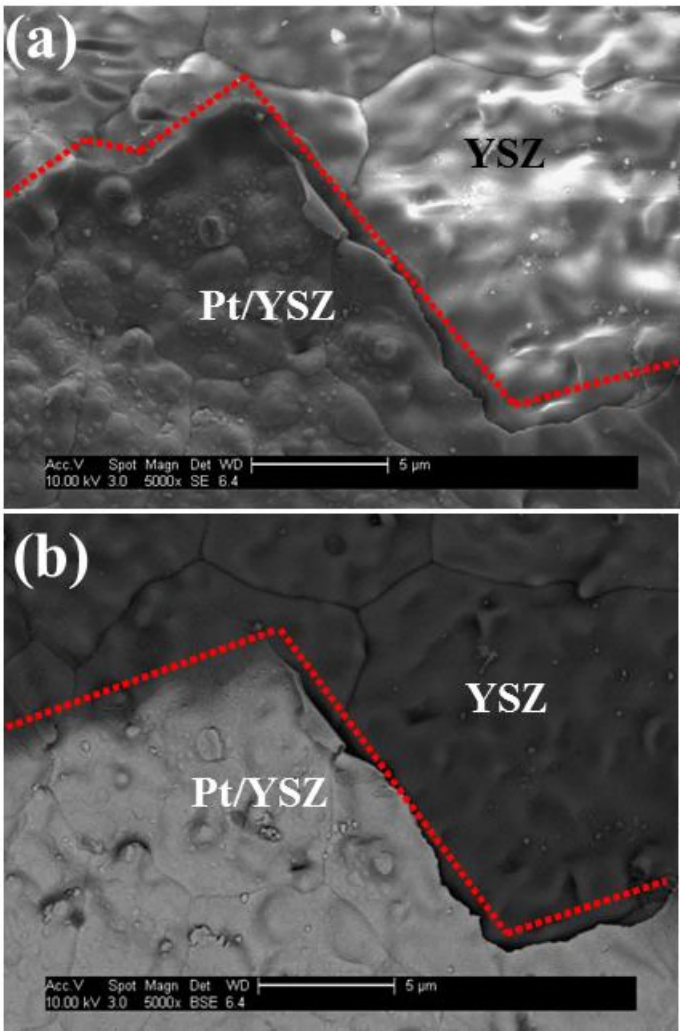

Figure S6. SEM images of the Pt(80)/YSZ after catalytic chemical reaction measurement. (a) secondary electron image; (b) back-scattered electron image from the same area shown in (a).

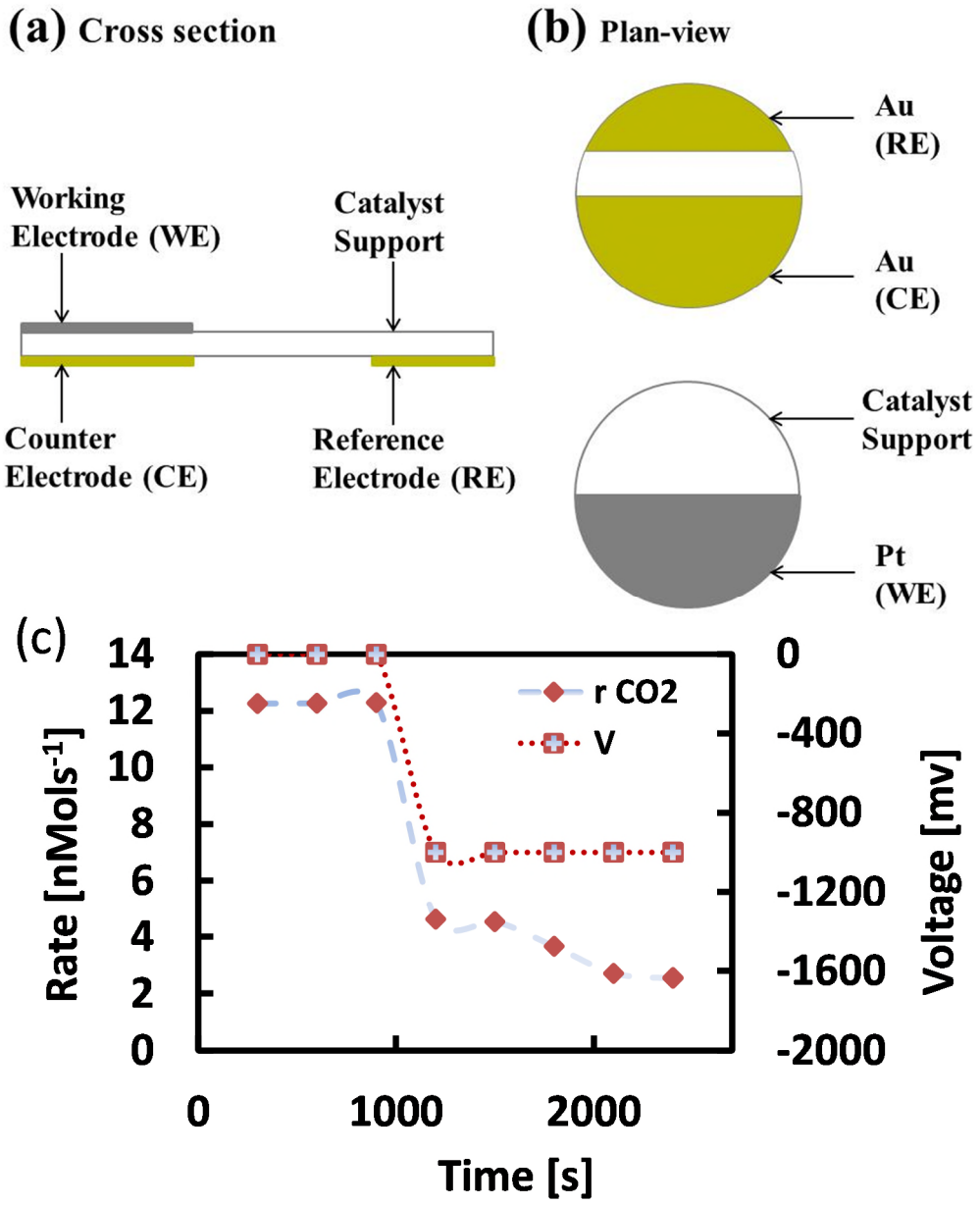

Figure S7. (a) Cross-sectional, and (b) plan view of electrodes for Non-Faradaic-electrochemical-modification-of-catalytic-activity (NEMCA) characterisation for Pt(80)/YSZ. (c) the ethylene oxidation reaction rate was reduced from 12.3 to 2.5 n mol s^{-1} when an external voltage of -1000 mV was applied to the Pt/YSZ. The working electrode was Pt, the reference and counter-electrode electrodes were Au.

Simulation and modelling: The modelling was built with eight layers of Pt on top of two unit cells of BCSO along XYZ directions, above Pt there were at least 1.5 nm of vacuum to ensure an accurate energy level for the vacuum to be obtained. First principle calculation was carried out using VASP (Vienna *ab initio* simulation package). The exchange-correlation term was described within the generalized gradient approximation (GGA) parameterized by Perdew-Burke-Ernzerh (PBE) functional.

For intrinsic semiconductor, the Fermi level is

$$E_i = \frac{E_c + E_v}{2} + \frac{3k_0T}{4}\ln\frac{m_p^*}{m_n^*} \qquad (S1)$$

the intrinsic carrier concentration is

$$n_i = \left[\frac{2(2\pi k_0T)^{3/2}(m_p^* m_n^*)^{3/4}}{h^3}\right]\exp(-\frac{E_g}{2k_0T}) \qquad (S2)$$

Here *h* is Planck's constant, E_c and E_v are the energy at the bottom of the conduction band, and maximum of the valance band, respectively. m_p^* and m_n^* are the effective mass for holes and electrons respectively, E_g the band gap. After the band structure has been obtained, the effective mass was obtained using

$$m^* = \hbar^2\left(\frac{\partial^2 E}{\partial k^2}\right)^{-1} \qquad (S3)$$

The so obtained m_p^* = 0.54 m_0, and m_n^*=0.23 m_0 (these values agree with those in references). [S1,S2] So, the term $\frac{3k_0T}{4}\ln\frac{m_p^*}{m_n^*}$ in equation (S1) is less than 0.02 eV，

which is negligible compared with E_g (0.80 eV). [S3] This indicates that the intrinsic Fermi level is in the middle of the band gap, and independent with temperature. The work function can be obtained as the difference between the energy of the vacuum and this Fermi level.

The Fermi level of a doped BCSO can be obtained using equation (S4),

$$E_f = E_i + k_0 T \cdot sh^{-1}(\frac{N_d}{2N_i}) \qquad (S4)$$

Charge transfer as a function of temperature is also calculated for Pt supported on a BCSO with donor concentration 10^{19} cm^{-3}. In this case, as the work function of Pt was much larger than the work function of the BCSO, the charge transfer made the interface area to become a charge depleted area in the semiconductor side, therefore form a contact barrier, and the bending of the energy band near the interface.

The amount of charge transferred upon the contact between Pt and BCSO can be calculated using equation (S5): [S4]

$$Q = e(N_d + n_i)W = [2\varepsilon_s e(N_d + n_i)|V0|]^{1/2} \qquad (S5)$$

Here N_d is the donor concentration, n_i the intrinsic carrier concentration, ε_s the dielectric constant, V_0 the difference in work function between the metal Pt and the semiconductor BCSO.

References

(S1) Yang, J.; Yang, G.; Zhang, G.; and Wang, Y., Low Effective Mass Leading To An Improved *ZT* Value By 32% For N-Type Bicuseo: A First-Principles Study, *J. Mater. Chemi.* **2014**, A2, 13923-13931.

(S2) Pei, Y. L.; He, J.; Li, J.; Liu, Q.; Pan, W.; Barreteau, C.; Berardan, D.; Dragoe, N.; and Zhou, L., High Thermoelectric Performance of Oxyselenides: Intrinsically Low Thermal Conductivity of Ca-doped BiCuSeO, *Npg Asia Material* **2013**, 5, 425-434.

(S3) Zakutayev, A.; Newhouse, P.; Kykyneshi, R.; Keszler, D.; and Tate, J., Pulsed Laser Deposition of BiCuOSe Thin Films, *Appl. Phys*. **2011**, A102, 485-492.

(S4) Ioannides, T. and Verykios, X., Charge Transfer in Metal Catalysts Supported on Doped TiO_2: A Theoretical Approach Based on Metal-Semiconductor Contact Theory, *J. Catal.* **1996**, 161*,* 560-569.

https://dspace.org/

In-situ tuning of catalytic activity by thermoelectric effect for ethylene oxidation

Achour, Abdenour; Liu, Jian; Peng, Ping; Shaw, Christopher; Huang, Zhaorong

2018-09-20
American Chemical Society
https://doi.org/10.1021/acscatal.8b02409
Abdenour Achour, Jian Liu, Ping Peng, et al., (2018) In-situ tuning of catalytic activity by thermoelectric effect for ethylene oxidation. ACS Catalysis, Volume 8, Issue 11, November 2018, pp. 10164-10172

Downloaded from a DSpace repository. https://dspace.org/